Robotica (2019) volume 37, pp. 338–357. © Cambridge University Press 2018
doi:10.1017/S0263574718001042

A modular bilateral haptic control framework for teleoperation of robots

Zeki Y. Bayraktaroglu†*, Omer F. Argin‡ and Sinan Haliyo§

†*Mechanical Engineering Department, Istanbul Technical University, Istanbul, Turkey*
‡*Mechatronics Engineering Department, Istanbul Technical University, Istanbul, Turkey.*
E-mail: oargin@itu.edu.tr
§*Sorbonne Université, CNRS, Institut des Systèmes Intelligents et de Robotique, ISIR, Paris, France.*
E-mail: sinan.haliyo@sorbonne-universite.fr

(Accepted September 17, 2018. First published online: October 30, 2018)

SUMMARY

This paper presents a novel approach to implement bilateral control loops between local haptic devices and remote industrial manipulators using a layer of simulation and virtual reality. The remote scene of manipulation has been visualized in an open-source software environment, where forward and inverse kinematics of the manipulators can be computed. Therefore, the explicit knowledge of mathematical models of the robots is not required for the implementation of the proposed bilateral control schemes. A haptic coupling has been designed between the human operator and the task in the remote environment. Virtually introduced force feedback has contributed to the performance of the proposed bilateral loop by facilitating the adaptation of unexperienced human operators. Teleoperation of one remote manipulator has been experimentally demonstrated with the proposed controllers. Structural modularity of the bilateral haptic control schemes makes them directly extendable for the teleoperation of multiple collaborative robots. Stability and transparency of the proposed bilateral haptic controllers have been theoretically and experimentally investigated.

KEYWORDS: Control of robotic systems; Haptic interfaces; Man-machine systems; Teleoperation; Bilateral control systems.

Nomenclature

K_x, K_f	Diagonal position and force scaling matrices for the output motion of the haptic interface and for the input force to the haptic interface.
K_i, B_i	Diagonal stiffness and damping matrices of the virtual spring model
m	Mass of the virtual spring-damper model.
$\underline{X}_H$	Cartesian coordinates commanded by the haptic interface/in Haptic frame.
$\underline{X}_{HS}$	Scaled coordinates commanded by the haptic interface/in Haptic frame.
$\underline{X}_T^r$	Cartesian coordinates commanded by the haptic interface/in Task frame.
$\underline{X}^r$	Reference Cartesian coordinates/in Task frame.
$\underline{X}^T$	Calculated end-effector position/in Task frame.
$\underline{q}^r$	Reference and measured joint positions vector/in Joint frame.
$\underline{e}_q$	Joint position errors vector/in Joint frame.
$\underline{e}_f$	Force errors vector/in Task frame.
$\underline{\tau}$	Joint torque vector/in Joint frame.
$\underline{f}_e$	External interaction forces vector/in Task frame.
$\underline{f}_T$	Measured end-effector force vector/in Task frame.

* Corresponding author. E-mail: zeki.bayraktaroglu@itu.edu.tr

$\underline{f}_C$	Coupling force vector/in Task frame.
$\underline{f}_{TF}$	Feedback force vector/in Task frame.
$\underline{f}_H$, $\underline{f}_{HS}$	Measured and scaled end-effector force vectors/in Haptic frame.
S_u, S_e	Stiffness' of the human operator and environment sides.
Z_u, Z_e	Impedances of the human operator and environment sides.

1. Introduction

Theoretical aspects of bilateral haptic controllers have been rigorously investigated in literature. Many bilateral schemes with various assumed operating conditions and controllers have been proposed and analyzed. Non-linearities in bilateral loops are generally introduced by the kinematics and dynamics of manipulators operating in remote environments. Linear techniques of stability analysis may apply in the case that the remote manipulator exhibits linear behavior.[1,2] Stability analysis of bilateral teleoperation systems incorporating non-linearities can be carried out in the general frame of the Lyapunov theory along with passivity approach.

Improvement of the stability and tranparency are the main challenges in bilateral teleoperation systems. Time delays on the communication channels have a disturbing impact on tracking performance and stability of bilateral teleoperation. Among earlier contributions, Anderson and Spong investigated the asymptotic stability and bilateral control of remote teleoperators.[3,4] Niemeyer and Slotine published contributions to fundamental issues of teleoperation with studies of adaptive control and force reflection.[5,6] Zhu and Salcudean,[7] Hashemzadeh *et al.*,[8] Sarras *et al.*,[9] Hou and Sourina[10] and Kim *et al.*[11] proposed adaptive control techniques for teleoperation systems with time delays. Smith predictor,[12,13] guaranteed cost control,[14] state convergence[15] and robust fixed-structure control[16] schemes are used to improve transparency in uncertain teleoperation systems with time-varying delays. Chopra *et al.* reported on tracking performance in bilateral teleoperation and problems related to communication networking.[17,18]

Lee and Spong investigated passive bilateral teleoperation and presented an experimental setup with a two-DoF direct-drive robot.[19] Nuño presented a teleoperation framework with an experimental setup including one haptic device and one remote manipulator.[20] Nuño *et al.* have shown that it is possible to control bilateral teleoperators with simple PD-like schemes with damping injection.[21] The analysis has been validated by simulations. In ref. [22], Nuño *et al.* proposed an experimental test-bed similar to that proposed in this work. The presented task consisted of moving the robot end-effector along a rail with a line restriction. Some intelligent force prediction methods have been used in variable time delayed bilateral systems. Li *et al.*[23–25] have proposed adaptive fuzzy and adaptive neural network controllers to compensate for time-varying delay. Lu *et al.*[26] have used predictive sensorless adaptive fuzzy controller and Zhao *et al.*[27] proposed augmented reality technology for real-time force reflection to improve stability and transparency.

Desbats *et al.* established force-feedback teleoperation in nuclear spent fuel processing application, using an industrial robot as the remote manipulator.[28] Soyguder and Abut proposed a modified wave variables method for the control of a single remote manipulator.[29] Shared control is mostly used in multilateral teleoperation systems.[30–32] Lu *et al.*[33] use multiple adaptive dominance factors in dual-user shared teleoperation system for enlarging the control flexibility.

Stability issues of bilateral systems involving single remote manipulator have been clearly presented with analysis results. A firm theoretical base has now been established for the analysis of bilateral haptic systems. A number of computer simulations of proposed bilateral control systems have been reported. Most of the published research deal with the case of bilateral haptic interaction with virtual environments. However, practical implementations of teleoperation systems in real remote environments are rarely present in scientific literature or in industrial applications.

This paper proposes a novel modular framework for the implementation of bilateral haptic coupling between one haptic device and one robot manipulator operating in remote environments. The aim of the proposed design is to establish a stable and robust teleoperation framework with user-friendly physical interfaces. Using an open-source simulation software in the loop, the coupling has been achieved with the sole knowledge of kinematic parameters of the remote manipulator. Experimental results confirm the flexibility of the proposed control system structure, which provides considerable ease in both implementation and remote operator handling.

https://doi.org/10.1017/S0263574718001042 Published online by Cambridge University Press

In the bilateral control system proposed in this paper, the haptic coupling is defined and computed in a layer of virtual reality environment, designed itself with an open-source software interface. There are two major contributions implemented within this layer of simulation and virtual reality. First, the remote physical environment has been virtually reconstructed and simulated to provide the human operator with a visual perception in real-time during teleoperation. The second contribution is about the virtual haptic coupling defined in the same simulation environment. Coupling forces computed in the virtual environment are added to the feedback forces measured at the remote interaction and the resulting total feedback force is applied to the haptic device. Feedback of virtual coupling forces felt by the human operator provides an additional tool, contributing to a better overall perception of the remote environment.

Robot controller gains are usually tuned to behave best around specific nominal motion dynamics, and there are always operational restrictions on joint accelerations. Unexperienced human operators have a tendency to apply highly dynamic motion inputs to the remote environment side, which may result with poor tracking performance and instability of the bilateral loop. Feedback of the virtually introduced coupling forces to the human operator makes him/her feel a resistance to the motion and helps improve the performance of the bilateral loop by preventing him/her from applying high-frequency motion inputs. The proposed haptic coupling design involving the virtual feedback forces introduces a low-pass filter behavior, filtering out high-frequency motion inputs from unexperienced human operators.

The main and secondary contributions of the proposed design to the performance of the teleoperation system is summarized as follows:

- The main contribution is the improvement of the stability of the bilateral loop, compared to a setup without the proposed coupling. Considering the nature of interaction between the user and haptic interface, improved stability would result in better tracking performance in the remote environment.
- The secondary contribution is the adaptation of unexperienced (untrained) users to the teleoperation system. Stability and robustness of the proposed bilateral coupling would help minimizing training periods of new users.

The challenges of this work are related to the design of the bilateral haptic controllers. A structurally simple design is aimed to achieve stable and transparent teleoperation. Corresponding requirements are described by the following design criteria:

- The bilateral control loop must rely on very minimal information about the remote manipulator: Only geometric/kinematic modeling is required.
- The controller structure of the remote manipulator must be as simple as possible: Basic PIDs are used for each joint control in a decentralized control approach.

In the following section, the bilateral haptic coupling used in the proposed control systems is presented. Motion control of remote manipulators as well as overall bilateral control schemes are presented in Section 3. Section 4 presents a Lyapunov-like analysis of the bilateral loop with a single remote manipulator, investigating the stability conditions. The hardware and software used in implementations as well as the control parameters are presented in Section 5. Experimental results of teleoperation of single remote manipulator are given in Section 6. Section 7 presents conclusions.

2. Bilateral Haptic Coupling with Virtual Spring-Damper Model

Haptic coupling design between distant physical devices can be defined based on the behavior of the haptic device present in the bilateral loop. Two main design approaches are based on the impedance and admittance of the haptic device, also called as the master or local device.

In the impedance approach, the master (local) device position is used as the motion reference for the slave (remote) manipulator. The slave-side force measurements are fed back to the haptic device, all with proper scaling factors. This kind of coupling is easily destabilized if different coefficients are used in force and motion scaling. Another limitation is that the user does not receive any information on the slave dynamics, except what is directly measured by a force/torque (F/T) sensor, usually mounted on the wrist of the remote manipulator.

In the admittance approach, the master device is controlled as to mimic the slave manipulator dynamics. Forces applied by the user to the haptic device are transmitted as references for the force

https://doi.org/10.1017/S0263574718001042 Published online by Cambridge University Press

control of the slave manipulator, and its motion is fed back as the motion reference for the haptic device. This kind of coupling requires F/T measurements at the master device. It should also be controlled in closed-loop to match the slave device's apparent mass, inertia and other mechanical behavior. This is considerably more complex, both for the hardware of the master device and identification of the slave manipulator.

As the overwhelming majority of the commercial haptic devices makes only impedance available, where an indirect coupling mode through a virtual viscoelastic element is generally used.[34] In this case, master and slave positions are each considered at opposite ends of a virtual spring-damper. Their relative motions deform this element. The resulting virtual force summed to the slave force sensor output is then used to force control the slave manipulator on one side and fed back to the user on the other. Tuning the stiffness and damping of this viscoelastic element allows for a compromise between the stability and transparency, and is reported to give satisfactory results. This indirect coupling strategy is largely inspired by a large corpus of works on physically based simulations with haptic interaction.[35,36] Several enhancements are studied, such as automatic tuning of the spring-damper parameters, or adaptive schemes.[37]

There are however several important differences in the implementation depending on the nature of the remote environment. In simulation applications where the remote scene is virtual, the haptic coupling is established between the master device and manipulated (virtual) object. In teleoperation applications where real physical interactions are controlled in remote environments, the coupling is defined between the master (haptic) device and the end-effector of the slave (remote) manipulator. Hence, the user feedback stems from the slave manipulator, but not the manipulated load. Moreover, force control of the slave side is often not straightforward and requires the knowledge and use of a dynamic model. Generally, only a single slave manipulator can be remotely operated without an elaborate scheme.

The framework presented here aims to establish haptic coupling in task space, between the master device and manipulated object (load) directly. The load may be handled by one or several collaborating remote manipulator(s). Consequently, dynamics of the remote manipulator is neglected in servo-control and the slave device is reduced to a simple motion transmitter, constituting a stand-alone component of the bilateral loop. In this modular approach, any robot whose basic kinematic parameters are available can serve as the remote manipulator.

The proposed framework is based on two simultaneous parallel couplings. A virtual reality and physical simulation environment is used as the middle layer, and includes the manipulated object and the remote manipulator. It provides real-time simulation of the dynamics, i.e. object motion is calculated from a set of forces, and inverse kinematics of the slave robot, considering the load as the goal position. Both those features are easily available, as open-source libraries or commercial products.

The first coupling, borrowing the conventional haptic physical simulation technique, is established between the haptic interface and virtual object using a spring-damper model. This generates a force to move the virtual object and gives haptic feedback about the object's simulated inertia to the user. Collisions or haptic guides can be easily added. The second coupling is between the end-effector of the remote manipulator handling the real object and the virtual object. This link is unilateral: the spring-damper force is only fed to the virtual object to reflect any position error on the real remote-side. The remote manipulator is controlled in joint space, with the configuration of the virtual slave robot as its motion references. Therefore, this second coupling generates information on the dynamics of the remote manipulator. This information can be augmented by an F/T sensor on the slave side.

Several contributions stem from this double coupling through the layer of simulation and virtual reality. The remote physical environment has been virtually reconstructed and simulated to provide the human operator with a visual perception in real time during teleoperation. If collision detection is provided by the simulator, it is very straightforward to implement safe zones, haptic guides, or other augmented visual or audio feedback.

From a perception perspective, the user receives a feedback related to both object's and the remote manipulators' motion and inertia. The ratio between the two can be easily tuned through homothetic coefficients on both couplings.

In the bilateral schemes proposed in this work, control of the remote manipulator is based on the sole knowledge of the basic kinematics, i.e. link lengths and joint definitions. The basic bilateral control scheme can be easily extended to the case of collaborating remote manipulators: a large load

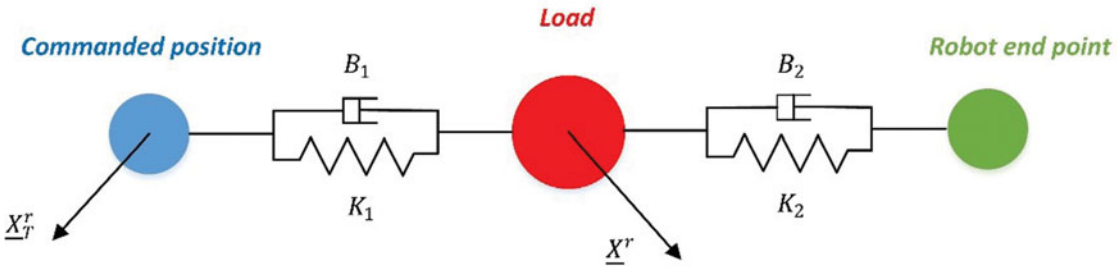

Fig. 1. Virtual spring-damper model.

to be manipulated at several points will have different handling points, each representing the goal of inverse kinematics problem of one slave manipulator. Hence, the user does not need to care about the trajectories of each manipulator, but only of the load itself. However, he will be constrained in his motion by the physical interaction and object dynamics through kinesthetic feedback. The human motor context is expected to deal with this situation quite well.

2.1. Virtual spring-damper model and total feedback force

The position references generated by the human operator through the haptic interface, after scaling, are denoted by $\underline{X}_T^r$ in task frame. A virtual spring-damper model is designed to achieve the transmission of the motion references to the robot controller as shown in Fig. 1. Haptic coupling forces are assumed to result from the interaction with this virtual spring-damper interface.

Dynamics introduced in the haptic loop is then given by the following equation:

$$m\ddot{\underline{X}}^r + B_2\dot{\underline{X}}^r + K_2\underline{X}^r = B_1\dot{\underline{X}}_T^r + K_1\underline{X}_T^r \tag{1}$$

The resulting haptic coupling force $\underline{f}_C$ and the total force $\underline{f}_{TF}$ to be applied to the haptic interface are written as follows:

$$\underline{f}_C = K_1\left(\underline{X}_T^r - \underline{X}^r\right) + B_1\left(\dot{\underline{X}}_T^r - \dot{\underline{X}}^r\right) \tag{2}$$

$$\underline{f}_{TF} = \underline{f}_C + \underline{f}_T \tag{3}$$

2.2. Bilateral haptic control system

The bilateral haptic control system for teleoperation proposed in this work is presented in Fig. 2. In this scheme, a human operator controls the motion of a remote robot through the proposed haptic coupling for manipulation purposes. Three main blocks representative of static and dynamic subsystems can be identified in this bilateral loop.

Scaling of motion and force signals are linear operations and establish static relationships between the operator-side and task environment-side variables.

The Blender,[38] an open-source software used as the main component of the bilateral loop, executes three tasks. First, the kinematic chain and parameters of the robot manipulator are defined in Blender's virtual environment, and the remote environment is visualized for the human operator. Second, the dynamic behavior of the virtual spring-damper model is simulated in Blender. Third, Blender computes the forward and inverse kinematics of the manipulator. Forward and inverse coordinate transformations define static mappings between joint and task space of the manipulator. Performance of these computational tasks by an extendable software environment contribute greatly to the compactness and simplicity of the proposed bilateral loop.

The remote robot, supposed to manipulate objects and interact with its environment is controlled in a feedback + feedforward loop with decentralized PIDs for each DoF. Dynamics of this subsystem can be modeled by non-linear equations of motion. Time delays in the communication channels are assumed to be constant.

https://doi.org/10.1017/S0263574718001042 Published online by Cambridge University Press

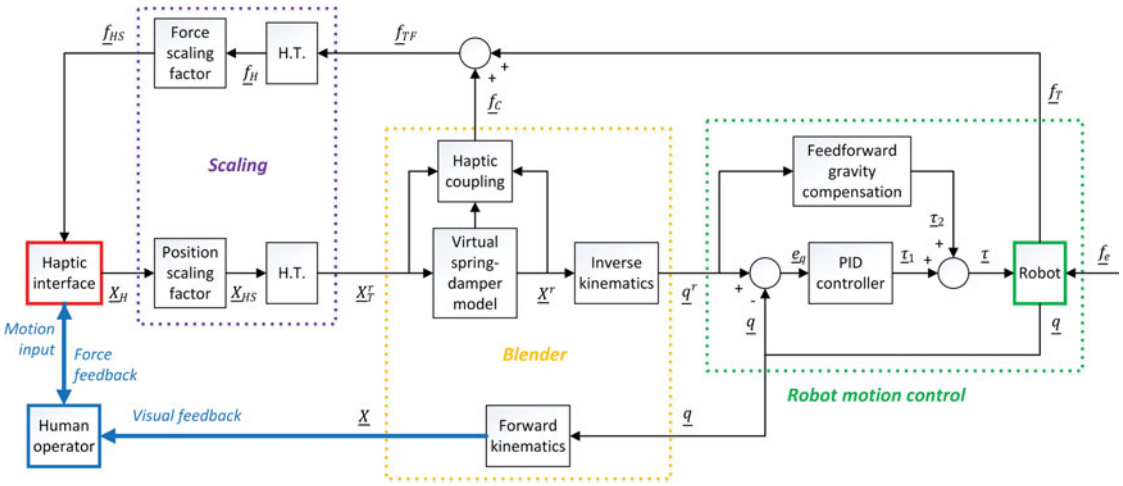

Fig. 2. Bilateral haptic coupling between one haptic device and one remote manipulator.

2.3. Position and force scaling

Workspaces of the haptic interfaces are generally reduced compared to those of industrial manipulators. Manipulation/interaction tasks may require larger workspaces than those of haptic devices. Therefore, the motion input provided by the haptic interface has to be amplified to be compatible with the physical task defined in the manipulator's workspace. Position scaling factor for the output motion of the haptic interface will be denoted by the (3×3) diagonal matrix K_x.

Amplitudes of interaction forces of the manipulators may depend on parameters related to the task to be achieved, such as the mass of an object to be manipulated. Amplitudes of continuous forces in haptic interfaces are generally less than 10 N. Therefore, the interaction forces measured with six-axis F/T transducers have to be scaled before being fed back to the haptic interfaces. Force scaling factor for the output motion of the haptic interface will be denoted by the (3×3) diagonal matrix K_f.

The use of diagonal matrices to set the position and force scaling factors allows the implementation of individually weighed scaling factors along the axis' of the world frame.

2.4. Forward and inverse coordinate transformations

Motion input provided by the human operator through the haptic interface is generated in task space and transmitted toward the environment through the virtual spring-damper model presented in Section 2.2. $\underline{X}_T^r$ is the (3×1) position vector representing the position only of the task space target point. The task space vector is then extended to the (6×1) position and orientation vector $\underline{X}^r$ such that the gripper remains in a constant orientation in task space.

The robot motion controller is itself implemented in joint space. Therefore, the task space references $\underline{X}^r$ have to be transformed into joint space references $\underline{q}^r$. The inverse kinematics of the manipulator is achieved in virtual (Blender) environment.

3. Robot Control

In this work, the experimental setup of the proposed teleoperation system has been established. The fundamental bilateral scheme (Fig. 2) describes the manipulation system with one haptic device and one remote manipulator.

In the haptic coupling presented in Section 2, one six-axis industrial manipulator is used to manipulate objects and interact with the environment. An independent joint control scheme with decentralized PIDs for the motion control of the manipulator is proposed.

Independent joint control schemes result in the simplest closed-loop structures possible for the motion control of manipulator arms. Although the dynamics of the remote manipulator is neglected, implementation of independent joint controllers are proven to be satisfactory in many applications with relatively slow and smooth motions. In the haptic coupling presented in Fig. 2, the default workspace of the robot is reduced and reference velocities and accelerations are generated by the

https://doi.org/10.1017/S0263574718001042 Published online by Cambridge University Press

human operator. The control signal is strengthened by the addition of a feedforward action for gravity compensation.

The robot control loop shown in Fig. 2 is based on independent joint controller with feedforward gravity compensation. The PID control law in joint space is given as follows:

$$\underline{\tau}_1(t) = K_p\left(\underline{e}_q(t) + \frac{1}{T_i}\int \underline{e}_q(\tau)\,\mathrm{d}\tau + T_d\frac{\mathrm{d}\underline{e}_q(t)}{\mathrm{d}t}\right) \tag{4}$$

where $\underline{e}_q = \underline{q}^r - \underline{q}$ is the joint position error, and K_p, T_i and T_d denote (6×6) diagonal matrices for the PID parameters.

The feedforward action compensating for the external torque $\underline{\tau}_2$ due to gravitational acceleration is calculated as a nonlinear function of the robot configuration, and the total input torque applied to the robot joints is given by

$$\underline{\tau} = \underline{\tau}_1 + \underline{\tau}_2 \tag{5}$$

The robot equations of motion can be written in standard form as follows:

$$A\left(\underline{q}\right)\ddot{\underline{q}} + C\left(\underline{q}, \dot{\underline{q}}\right)\dot{\underline{q}} + \underline{Q}\left(\underline{q}\right) = \underline{\tau} \tag{6}$$

where $A\left(\underline{q}\right)$ is the inertia matrix, $C\left(\underline{q}, \dot{\underline{q}}\right)$ is the matrix of Coriolis and centrifugal forces and $\underline{Q}\left(\underline{q}\right)$ is the torque vector due to gravity.

Lyapunov stability of the closed-loop dynamics given by Eqs. (5) and (6) has been proved with the following Lyapunov function:

$$V = \frac{1}{2}\cdot\dot{\underline{q}}^T A\dot{\underline{q}} + \frac{1}{2}\cdot\underline{e}_q{}^T K_p\underline{e}_q \tag{7}$$

Application of the invariant set theorem has shown the asymptotic stability of the closed-loop dynamics as given in refs. [39,40].

4. Stability and Transparency of the Bilateral Haptic Loop

4.1. Stability

Stability of bilateral teleoperation has been investigated by Nuño *et al.* in refs. [20–22, 41, 42] and by Hua in ref. [43]. In ref. [20], a general theoretical framework allowing the stability analysis of various control schemes presented in the literature is proposed. The framework is based on the Lyapunov stability theory with passivity-based formulations. A comparative analysis of performances of different controllers shows that bilateral loops with PID type controllers are robust in presence of variable time delays and exhibit stable bilateral coupling. Time delays may have important influence on the loop stability. Stability of bilateral loops with constant and variable time delays has been investigated as well in refs. [20,41–43]. Stability analysis presented in this section follows a similar approach as given in above-mentioned publications. The haptic coupling between one haptic device and a single remote manipulator as presented in Fig. 2 is considered in the following analysis.

4.1.1. Properties and assumptions. Based on the equations of motion of robot manipulators as given in Eq. (6), closed-loop dynamics of the bilateral haptic control system proposed in this work can be represented as follows:

$$A_m\left(\underline{q}_m\right)\ddot{\underline{q}}_m + C_m\left(\underline{q}_m, \dot{\underline{q}}_m\right)\dot{\underline{q}}_m = \underline{\tau}_m - \underline{\tau}_{\text{user}} \tag{8}$$

$$A_b\left(\underline{q}_b\right)\ddot{\underline{q}}_b + C_b\left(\underline{q}_b, \dot{\underline{q}}_b\right)\dot{\underline{q}}_b = \underline{\tau}_b \tag{9}$$

https://doi.org/10.1017/S0263574718001042 Published online by Cambridge University Press

$$A_s\left(\underline{q}_s\right)\ddot{\underline{q}}_s + C_s\left(\underline{q}_s, \dot{\underline{q}}_s\right)\dot{\underline{q}}_s + \underline{Q}_s\left(\underline{q}_s\right) = \underline{\tau}_s + \underline{f}_e \tag{10}$$

In above equations (8)–(10), indices m, b and s denote the master haptic device, virtual Blender model and slave (remote) manipulator, respectively. $\underline{f}_e$ is the vector of interaction force between the remote manipulator and environment, and $\underline{\tau}_{\text{user}}$ is the F/T applied by the user through the haptic interface.

In the bilateral loop proposed in this work, communication delays are assumed to be constant valued and defined as follows:

- T_1: time delay between the haptic device and virtual model.
- T_2: time delay between the virtual model and remote manipulator.
- T_3: time delay between the haptic device and remote manipulator.

Control inputs to be applied to the master and slave manipulators are given as follows:

$$\underline{\tau}_m = K_m\left(\underline{q}_m - \underline{q}_b(t - T_1)\right) + B_m\left(\dot{\underline{q}}_m - \dot{\underline{q}}_b(t - T_1)\right) + \underline{f}_e(t - T_3) \tag{11}$$

$$\underline{\tau}_s = K_s\left(\underline{q}_b(t - T_2) - \underline{q}_s\right) + B_s\left(\dot{\underline{q}}_b(t - T_2) - \dot{\underline{q}}_s\right) + \underline{Q}_s\left(\underline{q}_s\right) \tag{12}$$

Assumptions on the parameters of robot manipulators are represented by the following mathematical properties:

- (P1) $A\left(\underline{q}\right)$ is a symmetric positive definite inertia matrix and there are positive constants r_1 and r_2 such that $r_1 I \geq A\left(\underline{q}\right) \geq r_2 I$.
- (P2) For all $q_i,\ x,\ y \in R^{n\times 1}$, there are positive scalars p_i such that $p_i \|x\| \|y\| \geq \|C_i(q_i, x)y\|$.
- (P3) There are positive scalars β_i such that $U_i(q_i) \geq \beta_i$, where $U_i(q_i)$ represents the potential energy of the robot, satisfying $g_i(q_i) = \partial U_i(q_i)/\partial q_i$.
- (P4) $\dot{A}_i\left(\underline{q}_i\right) = C_i\left(\underline{q}_i\right) + C_i{}^T\left(\underline{q}_i\right)$.

Lemma 1 (ref. [43]). *For a positive-definite matrix Υ, the following inequality holds:*

$$2a^T(t)\int_{t-T}^{t} b(\sigma)\,d\sigma - \int_{t-T}^{t} b^T(\sigma)\,\Upsilon\, b(\sigma)\,d\sigma \leq \overline{T}\,a^T(t)\,\Upsilon^{-1}a(t) \tag{13}$$

where $a(t)$ and $b(t)$ are vector functions and T is a time-varying scalar satisfying $0 \leq T \leq \overline{T}$.

Passivity of the human operator and environment can be represented by the following inequalities:

$$-\int_0^t \dot{\underline{q}}_m{}^T(\sigma)\,\underline{\tau}_{\text{user}}(\sigma)\,\mathrm{d}\sigma \geq 0, \qquad -\int_0^t \dot{\underline{q}}_s{}^T(\sigma)\underline{f}_e(\sigma)\mathrm{d}\sigma \geq 0 \tag{14}$$

4.1.2. Lyapunov stability. If the system given by Eqs. (8)–(10) is controlled through the inputs proposed in Eqs. (11) and (12) with the following bounds on $\underline{\tau}_b$ and $\underline{\tau}_{\text{user}}$:

$$\underline{\tau}_b \geq K_m(\underline{q}_m - \underline{q}_s), \quad \underline{\tau}_{\text{user}} \geq \frac{1}{2}\underline{f}_e(t - T_3) \tag{15}$$

https://doi.org/10.1017/S0263574718001042 Published online by Cambridge University Press

then $\dot{\underline{q}}_i$ and $\underline{q}_m - \underline{q}_s$ are shown to be bounded with the following Lyapunov function candidtate:

$$\begin{aligned} V = {} & \dot{\underline{q}}_m{}^T A_m\left(\underline{q}_m\right)\dot{\underline{q}}_m + \dot{\underline{q}}_b{}^T A_b\left(\underline{q}_b\right)\dot{\underline{q}}_b + \frac{K_m}{K_s}\dot{\underline{q}}_s{}^T A_s\left(\underline{q}_s\right)\dot{\underline{q}}_s + 2\left(U_m\left(\underline{q}_m\right) - \beta_m\right) \\ & + 2\left(U_s\left(\underline{q}_s\right) - \beta_s\right) + K_m(\underline{q}_b - \underline{q}_m)^2 - 2\int_0^t (\dot{\underline{q}}_m{}^T(\sigma)\,\underline{\tau}_{\text{user}}(\sigma) + \frac{K_m}{K_s}\dot{\underline{q}}_s{}^T(\sigma)\underline{f}_e(\sigma))\mathrm{d}\sigma \\ & + \frac{K_m}{K_s}K_s(\underline{q}_b - \underline{q}_s)^2 - B_m\int_{t-T_1}^t \left|\dot{\underline{q}}_b(\theta)\right|^2 \mathrm{d}\theta + \frac{K_m}{K_s}B_s\int_{t-T_2}^t \left|\dot{\underline{q}}_b(\theta)\right|^2 \mathrm{d}\theta \\ & + \int_{-\overline{T}_1}^0\int_{t+\theta}^t \dot{\underline{q}}_b{}^T(\sigma)\,S\dot{\underline{q}}_b(\sigma)\,\mathrm{d}\sigma\,\mathrm{d}\theta + \int_{-\overline{T}_2}^0\int_{t+\theta}^t \dot{\underline{q}}_b{}^T(\sigma)\,Z\dot{\underline{q}}_b(\sigma)\,\mathrm{d}\sigma\,\mathrm{d}\theta \end{aligned} \tag{16}$$

where S and Z are positive definite symmetric matrices.

Proof of the Lyapunov stability is given in Appendix.

4.1.3. Asymptotic stability. Since the proposed bilateral loop is a time-varying system, in order to prove the asymptotic stability of the bilateral loop in presence of negative semi-definite only $\dot{V}$, one has to show the uniform continuity of $\dot{V}$. According to Barbalat's Lemma,[44] uniform continuity of $\dot{V}$ implies the convergence $\dot{V} \to 0$ as $t \to \infty$.

In order to prove the uniform continuity of $\dot{V}$, its time-derivative must be shown to be bounded:

$$\begin{aligned} \ddot{V} = {} & 2\ddot{\underline{q}}_m{}^T\left(\overline{T}_1 K_m{}^2 S^{-1} + B_m\right)\dot{\underline{q}}_m + 2\ddot{\underline{q}}_b{}^T\left(\overline{T}_1 S + \overline{T}_2 Z + \frac{K_m}{K_s}B_s - B_m\right)\dot{\underline{q}}_b \\ & + 2\ddot{\underline{q}}_s{}^T\left(\overline{T}_2 K_m{}^2 Z^{-1} - \frac{K_m}{K_s}B_s\right)\dot{\underline{q}}_s + 2\ddot{\underline{q}}_m{}^T(\underline{f}_e(t - T_3) - 2\underline{\tau}_{\text{user}}) \\ & + 2\dot{\underline{q}}_m^T((1 - \dot{T}_3)\,\underline{\dot{f}}_e(t - T_3) - 2\underline{\dot{\tau}}_{\text{user}}) + 2\ddot{\underline{q}}_b{}^T(K_m\left(\underline{q}_m - \underline{q}_s\right) + \underline{\tau}_b) \\ & + 2\dot{\underline{q}}_b^T(K_m\left(\dot{\underline{q}}_m - \dot{\underline{q}}_s\right) + \underline{\dot{\tau}}_b) \end{aligned} \tag{17}$$

Based on closed-loop dynamics Eqs. (8) and (10), and control laws (11) and (12), joint accelerations of the master and slave manipulators are given as follows:

$$\begin{aligned} \ddot{\underline{q}}_m = {} & A_m{}^{-1}\left(K_m\left(\underline{q}_m - \underline{q}_b(t - T_1)\right) + B_m\left(\dot{\underline{q}}_m - \dot{\underline{q}}_b(t - T_1)\right) + \underline{f}_e(t - T_3)\right) \\ & + A_m{}^{-1}\left(-C_m\dot{\underline{q}}_m - \underline{\tau}_{\text{user}}\right) \end{aligned} \tag{18}$$

$$\ddot{\underline{q}}_b = A_b{}^{-1}\left(\underline{\tau}_b - C_b.\dot{\underline{q}}_b\right) \tag{19}$$

$$\ddot{\underline{q}}_s = A_s{}^{-1}\left(K_s\left(\underline{q}_b(t - T_2) - \underline{q}_s\right) + B_s\left(\dot{\underline{q}}_b(t - T_2) - \dot{\underline{q}}_s\right) - C_s\dot{\underline{q}}_s + \underline{f}_e\right) \tag{20}$$

Boundedness of $\underline{q}_i$, $\dot{\underline{q}}_i$, $\underline{f}_e$ and $\underline{\tau}_b$ in Eqs. (18) and (20) along with (P1) imply that of $\ddot{\underline{q}}_i$. The first three terms of $\ddot{V}$ are therefore bounded. Boundedness of the remaining four terms of $\ddot{V}$ is guaranteed according to conditions given in Eqs. (14) and (15).

Therefore, according to Barbalat's lemma, the proposed bilateral haptic system is shown to be asymptotically stable.

4.2. Transparency

Proceeding as in refs. [1] and [2], the definition of the transparency of the haptic coupling is based on impedances or stiffness' at the human operator and environment sides, as proposed in refs. [45]

https://doi.org/10.1017/S0263574718001042 Published online by Cambridge University Press

Fig. 3. Remote manipulators.

and [46]. Perfect transparency in a bilateral haptic loop is assumed to be achieved when both side impedances (or stiffness') are equal. Impedances and stiffness felt by the human operator (Z_u and S_u) and of the environment (Z_e and S_e) are defined as follows:

$$Z_u = \frac{\left\|\underline{f}_{HS}\right\|}{\left\|\underline{V}_H\right\|}, \quad S_u = \frac{\left\|\underline{f}_{HS}\right\|}{\|X_H\|}, \quad Z_e = \frac{\left\|\underline{f}_{TF}\right\|}{\left\|\underline{V}\right\|}, \qquad S_e = \frac{\left\|\underline{f}_{TF}\right\|}{\left\|\underline{X}\right\|} \tag{21}$$

These impedances and stiffness' have been calculated according to definitions (21), based on force and motion measurements.

5. Implementation

5.1. Hardware and software

The haptic interface of the proposed bilateral coupling is a Phantom Premium 1.5 High Force device. The haptic coupling has been implemented with a six-axis Stäubli Rx160 manipulator arm (Fig. 3). The manipulator is equipped with a six-axis ATI F/T transducers and a single-DoF on/off gripper. The robot motion control is implemented through the Low Level Interface provided in ref. [47]. Sampling frequencies of the robot controller and the haptic interface are 250 Hz and 1 kHz, respectively.

The dynamic behavior of the virtual spring model proposed in Section 2 as well as the inverse coordinate transformations are handled by an open-source 3D creation software.[38] Once the kinematic chains of the manipulator arms are defined in the graphical interface of the Blender software, forward and inverse kinematics are computed by appropriate solvers (Fig. 4).

Blender also comes with a physics engine, with which the dynamics of the manipulation and physical interactions can be simulated. The objects manipulated in experiments have been defined in Blender's interface (Fig. 5).

The purpose of the use of virtual environment in the proposed bilateral coupling system lies in the simplicity and modularity of the bilateral loop design. Kinematic parameters of the manipulator arm as well as the parameters of the virtual spring model can be easily modified through the Blender's graphical interface. In the case of the manipulator being replaced by another one, the use of virtual environment offers a user-friendly redesign of the bilateral loop.

https://doi.org/10.1017/S0263574718001042 Published online by Cambridge University Press

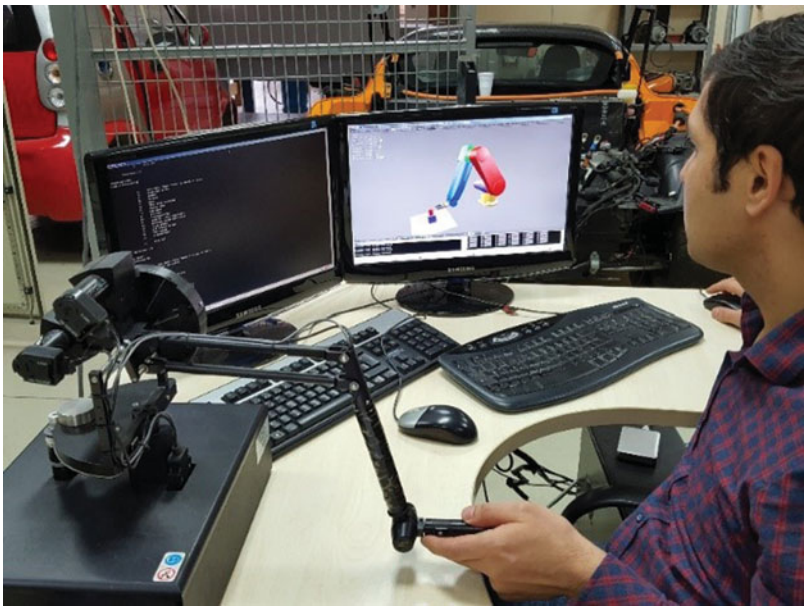

Fig. 4. Haptic device and virtual interface.

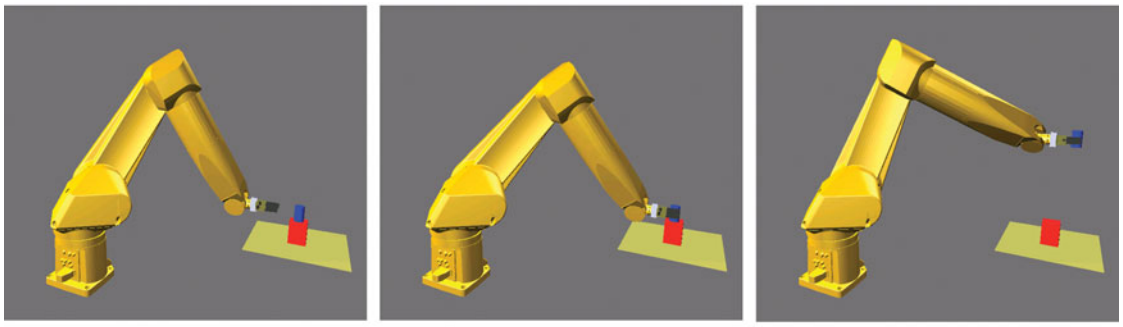

Fig. 5. Remote manipulator in the virtual (Blender) environment. (a) Approach phase. (b) Handling of the object. (c) Manipulation.

5.2. Control parameters

Parameters of the bilateral loop belong to three subsystems shown in Fig. 2: Scaling, Blender and Robot motion control.

5.2.1. Scaling factors. The position and force scaling factors $K_x = \frac{X_{HS}}{X_H}$ and $K_f = \frac{f_{HS}}{f_H}$ are determined according to the constraints related to the haptic device. The workspace of the haptic device is smaller than the robot's workspace and the sub-(work)space in which the robot operates depends on the task. The position scaling is then chosen so as to establish a convenient correspondence between these workspaces.

Choice of the force scaling depends primarily on the maximum force available on the haptic device. The maximum force of the haptic device has a limited value with respect to interaction forces that may occur in the physical environment. Accuracy of the F/T transducer being variable over a range of measured amplitudes, displays decisive effects on the quality of force feedback. The experiments have been planned such that the interaction forces in the remote environment remain close to the linear range of the F/T transducer. The force scaling is then chosen to obtain realistic force feedback without violating the capacity of the haptic device.

5.2.2. Virtual spring-damper and robot controller parameters. Stiffness and damping parameters of the virtual spring model presented in Section 2 have been determined for desired damping ratio ζ_d.

https://doi.org/10.1017/S0263574718001042 Published online by Cambridge University Press

Table I. Robot PID parameters.

Joint	K_p	T_d	T_i
1	3500	0.2	150
2	8000	0.04	250
3	6500	0.02	250
4	2500	0.025	40
5	1000	0.025	30
6	1000	0.01	30

Damping ratios satisfying $0,7 \leq \zeta_d \leq 1$ have been implemented in the experiments. Parameters have been selected such that the resulting natural frequency ω_n remains far from the structural frequencies of the haptic device. Note that stiffer springs will contribute to better position tracking but will result in higher coupling forces, which will in turn induce oscillations in system signals.

Finally, the PID parameters K_p, T_i and T_d of the robot controller given in Eq. (4) have been experimentally tuned (see Table I).

6. Experiments

In the experiments, haptic manipulation of rigid objects has been achieved with one remote manipulator. The bilateral control loop applied in the experiments is the one given in Fig. 2. The manipulated object has mass $m_l = 2$ kg and scaling factors have been implemented as follows: $K_x = 30,\ K_f = \frac{1}{30}$.

Parameters of the virtual spring-damper model have been implemented as follows: $m = 1,\ B_2 = 35$ and $K_2 = 600$. These values of the virtual model parameters result in a damping ratio of $\zeta = 0.714$ and a natural frequency $\omega_n = 24.5$ rad/s. The UDP/IP protocol is used in all communications between the master side (haptic interface), virtual robot (blender model) and slave side (remote manipulator). Experimentally, observed time delays are as follows: $T_1 = 0.7 - 0.8$ ms, $T_2 = 0.14 - 0.16$ ms, $T_3 = 0.7 - 0.8$ ms. The sampling frequency of the robot controller being 250 Hz, these time delays correspond to up to 20% of one sampling period with T_1 and T_3, and up to 40% with T_2.

The experimental task whose results are presented here consists of the following successive steps: (1) approach of the manipulator's end-effector to the load position, (2) handling of the load by the gripper, (3) manipulation of the load in a 3D region in the manipulator workspace, (4) release of the load to its initial position.

Tracking performance of the remote manipulator in task space is depicted in Fig. 6. The average position tracking error is 3.46 mm. Figure 7 shows the remote manipulator's measured and scaled end-effector forces by the scaling factor $K_f = \frac{1}{30}$.

The virtual spring force given in Fig. 8(a) is artificially introduced to the control loop and provides the user with an apparent inertia feeling while commanding the remote manipulator. Figure 8(b) depicts the total haptic feedback force applied to the haptic device interface, with the contributions of forces due to the haptic coupling and manipulated load, given respectively, in Figs. 7(b) and 8(a).

Figures 9 and 10 show the stiffness' and impedances calculated for the manipulator end-effector and haptic device. Since the implemented scaling factors satisfy $K_x.K_f = 1$, similar order of magnitudes as well as trends for stiffness' and impedances are observed at both ends of the bilateral loop as expected.

Experimental results presented in Figs. 6 to 10 have been obtained with an experienced user in the loop. The proposed bilateral control system has also been experimented on by unexperienced users. At the experiments with untrained users in the loop, similar behaviors have been observed in terms of fundamental performance criteria such as stability, transparency and position tracking in task space.

Figure 11 presents the tracking error performances with one experienced (trained) user and six unexperienced users. The average tracking error with the trained user is measured as 3.46 mm. The average of tracking errors with six untrained users is 4.01 mm.

The position tracking performance of the bilateral haptic loop is also evaluated in terms of the contribution of the proposed virtual reality layer. Figure 12 gives the position tracking errors measured with and without the use of the virtual force feedback, with a trained user in the loop. In the latter

https://doi.org/10.1017/S0263574718001042 Published online by Cambridge University Press

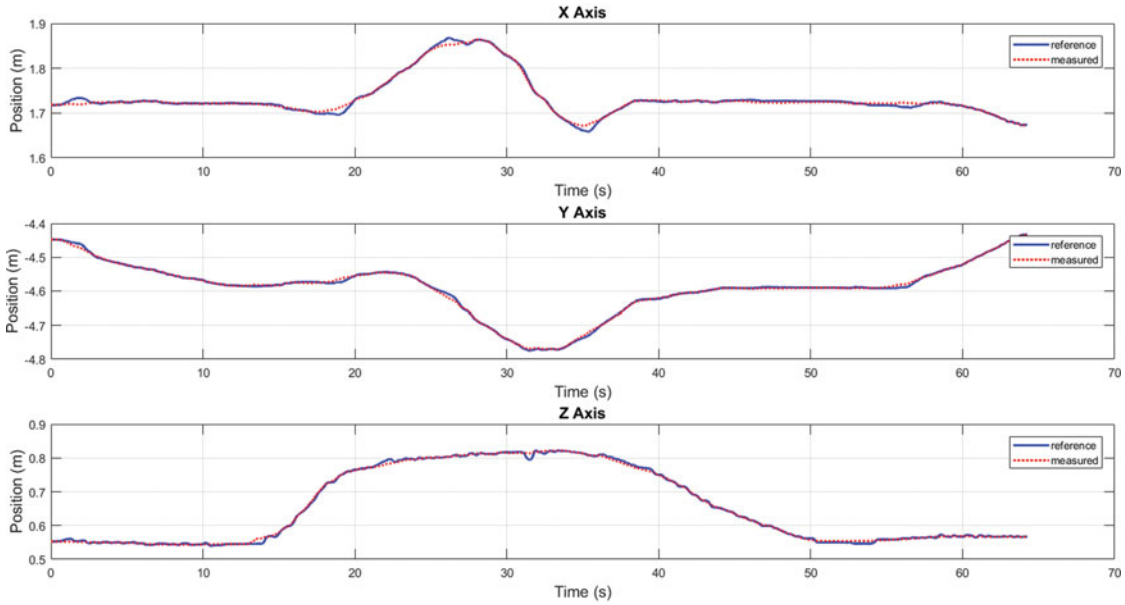

Fig. 6. Remote manipulator's position tracking in task space.

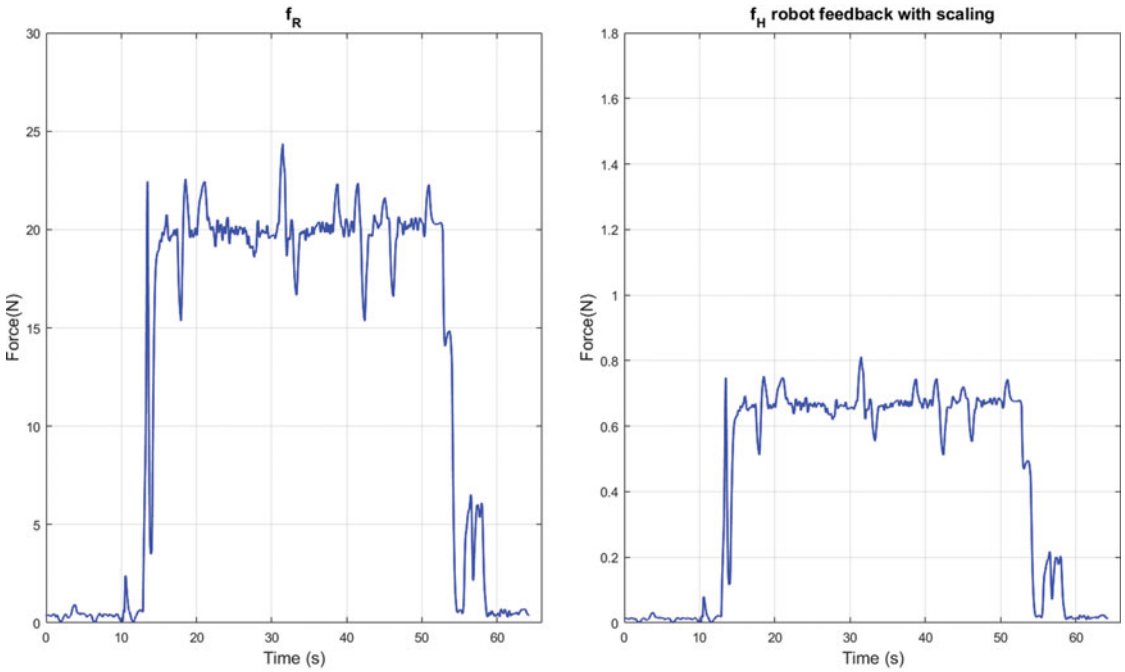

Fig. 7. Remote manipulator's (a) measured and (b) scaled end-effector forces.

case, the end-effector force measured (and scaled) at the remote scene is directly fed back to the haptic interface. The average tracking error without the virtual force feedback is 5.24 mm, whereas it was 3.46 mm with the contribution of the virtual force feedback, as presented in Fig. 11.

7. Conclusion

A novel bilateral haptic control loop between one haptic device and one remote manipulator is proposed in this paper.

https://doi.org/10.1017/S0263574718001042 Published online by Cambridge University Press

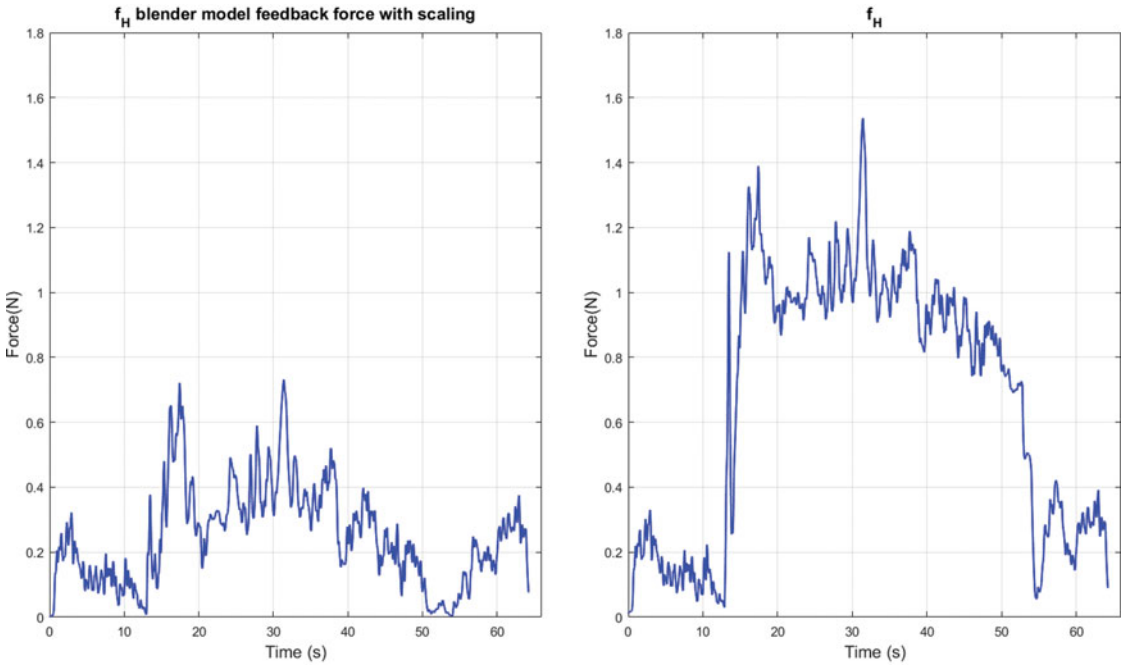

Fig. 8. (a) Virtual spring force. (b) Total haptic feedback force.

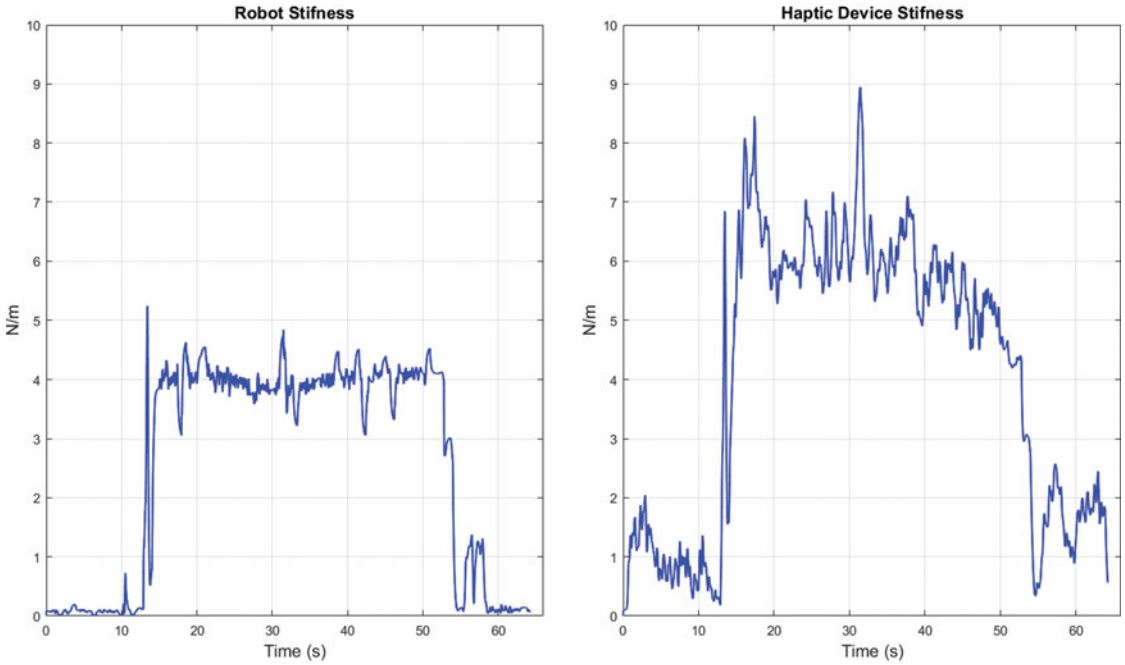

Fig. 9. (a) Remote manipulator. (b) Haptic device stiffness'.

Asymptotic stability conditions for the bilateral loop with a position controlled remote manipulator is theoretically investigated. With the implementation of the proposed controller, stable teleoperations are experimentally achieved by trained and untrained users. Transparency of the proposed bilateral loop is also experimentally evaluated as presented in Section 6.

Implementation and experimental validation of the proposed controller are achieved in a modular programming environment. Note that the proposed bilateral control scheme can be easily extended to collaboration tasks with multiple remote manipulators.

https://doi.org/10.1017/S0263574718001042 Published online by Cambridge University Press

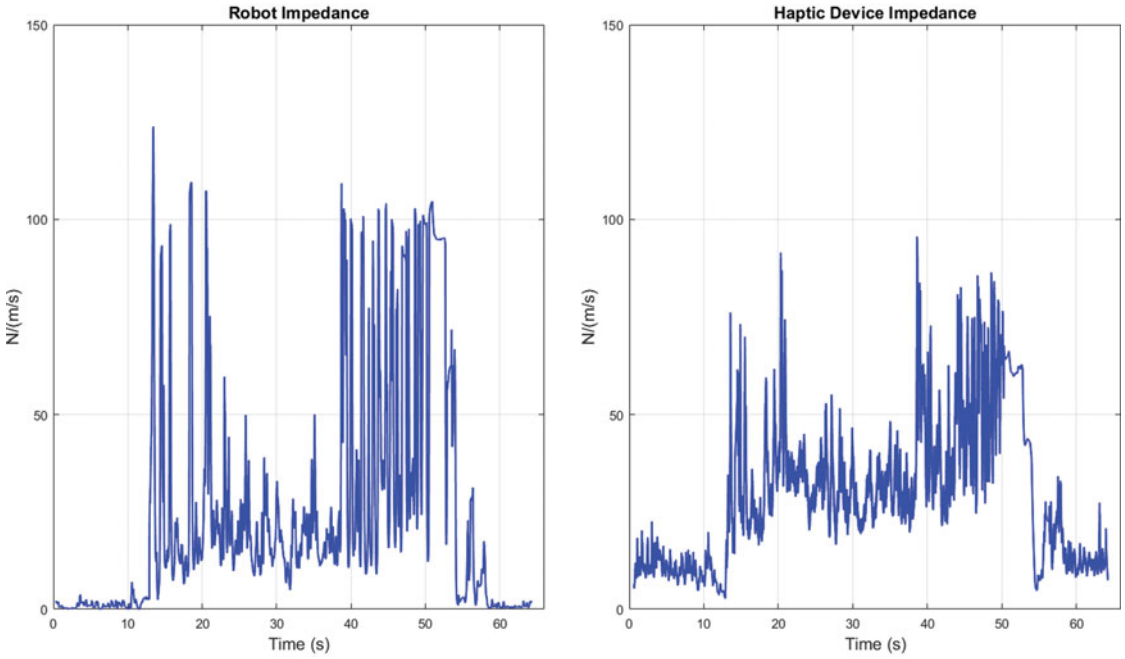

Fig. 10. (a) Remote manipulator. (b) Haptic device impedances.

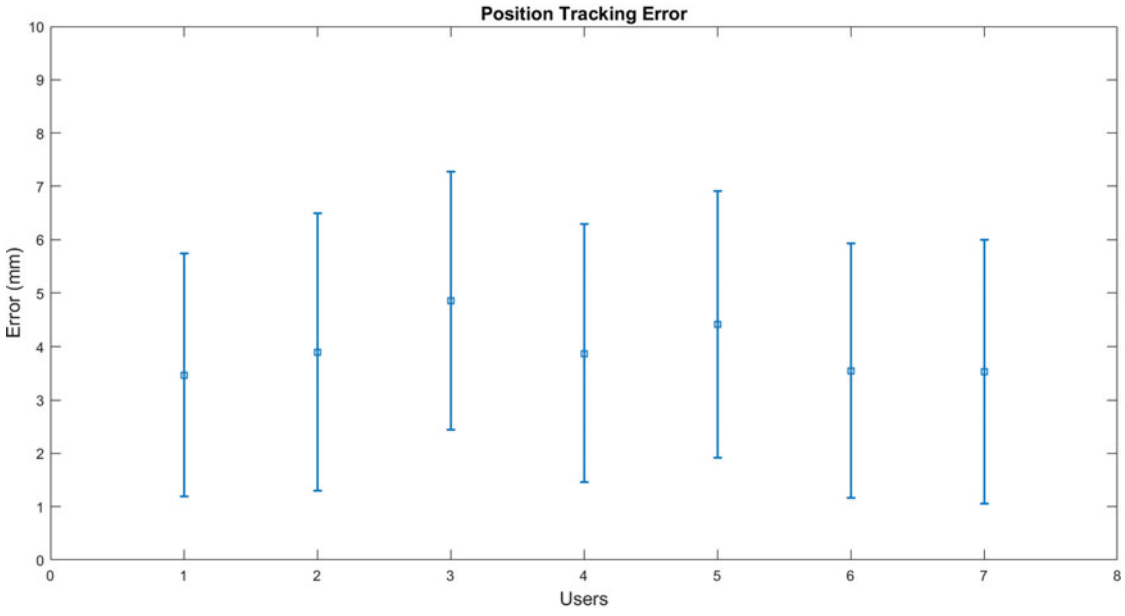

Fig. 11. Bounds of position tracking errors with one trained (first user) and six untrained users.

Definition of the kinematic chain involving geometric parameters of the manipulator is sufficient for the implementation of the proposed bilateral controllers. Since no further mathematical model is needed, any arbitrary robot arm whose geometric parameters are available can be easily integrated as the remote manipulator in the bilateral loop.

In position control of industrial manipulators, motion references with excessive accelerations may result in unstable behavior of the system, and the actuator currents are usually limited for safety reasons. In the absence of any haptic interface, motion references from the human operator side may exceed the allowable input frequencies. Then proper operation of the bilateral control system would require training periods of the users. The haptic coupling proposed in this paper provides the user with a feeling of apparent inertia during teleoperation. This artificially introduced

https://doi.org/10.1017/S0263574718001042 Published online by Cambridge University Press

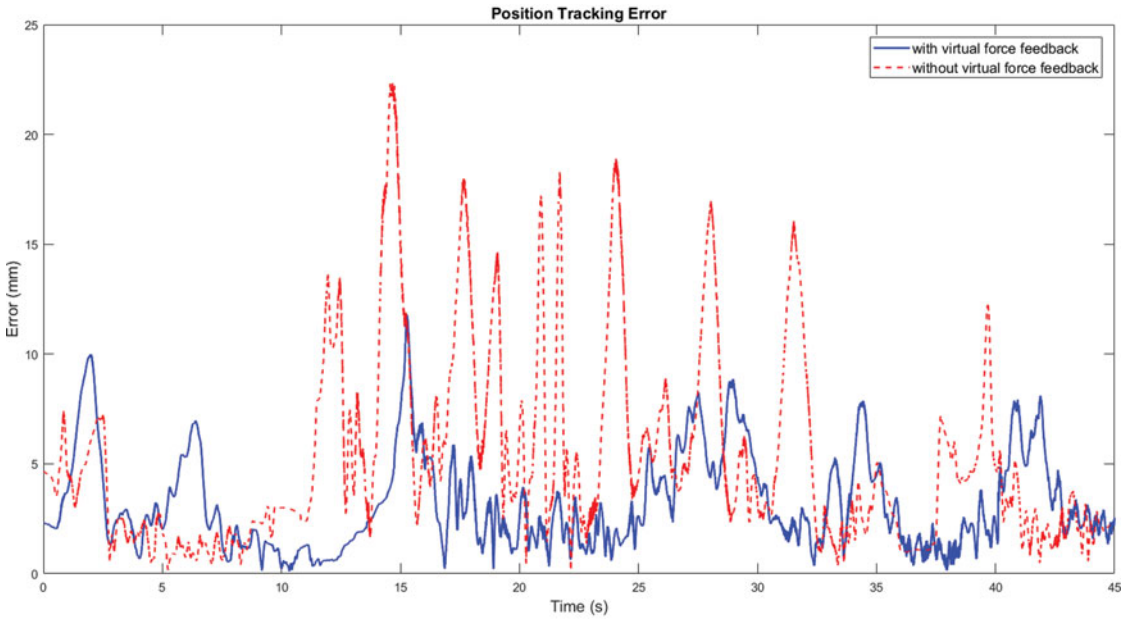

Fig. 12. Position tracking errors with and without virtual force feedback.

second-order dynamics filters out the high-frequency motion references from the user and therefore allows unexperienced users to easily achieve teleoperation. Experimental results presented here confirm the predicted contributions of the proposed haptic coupling.

Supplementary Material

To view supplementary material for this article, please visit https://doi.org/10.1017/S0263574718001042.

References

1. A. Bolopion, B. Cagneau, D. Haliyo and S. Régnier, "Analysis of stability and transparency for nanoscale force feedback in bilateral coupling," *J. Micro-Nano Mechatron.* **4**(4), 145–158 (2008).
2. A. Mohand Ousaid, A. Bolopion, S. Haliyo, S. Régnier and V. Hayward, "Stability and Transparency Analysis of a Teleoperation Chain for Microscale Interaction," *Proceedings of the IEEE International Conference on Robotics and Automation* (2014) pp. 5946–5951.
3. R. J. Anderson and M. W. Spong, "Asymptotic Stability for Force Reflecting Teleoperators with Time Delay," *Proceedings of the IEEE International Conference on Robotics and Automation* (1989) pp. 1618–1625.
4. R. J. Anderson and M. W. Spong, "Bilateral control of teleoperators with time delay," *IEEE Trans. Automat. Control* **34**(5), 494–501 (1989).
5. G. Niemeyer and J. J. E. Slotine, "Stable adaptive teleoperation," *IEEE J. Ocean. Eng.* **16**(1), 152–162 (1991).
6. G. Niemeyer and J. J. E. Slotine, "Transient Shaping in Force Reflecting Teleoperation," *Proceedings of the International Conference on Advanced Robotics* (1991) pp. 261–266.
7. W. H. Zhu and S. E. Salcudean, "Teleoperation with Adaptive Motion/Force Control," *Proceedings of the IEEE International Conference on Robotics and Automation* (1999) pp. 231–237.
8. F. Hashemzadeh, T. Hassanzadeh, M. Tavakoli and G. Alizadeh, "Adaptive control for state synchronization of nonlinear haptic telerobotic systems with asymmetric varying time delays," *J. Intell. Robot. Syst.* **68**(3), 245–259 (2012).
9. I. Sarras, E. Nuño and L. Basañez, "An adaptive controller for nonlinear teleoperators with variable time-delays," *J. Franklin Inst.* **351**(10), 4817–4837 (2014).
10. X. Hou and O. Sourina, "Real-time adaptive prediction method for smooth haptic rendering," Cornell University Library, preprint arXiv 1603.06674 (2016).
11. B.-Y. Kim and H.-S. Ahn, "A design of bilateral teleoperation systems using composite adaptive controller," *Control Eng. Pract.* **21**(12), 1641–1652 (2013).
12. A. Alfi and M. Farrokhi, "A simple structure for bilateral transparent teleoperation systems with time delay," *J. Dyn. Syst., Meas. Control* **130**(4), 044502 (2008).
13. A. Alfi and M. Farrokhi, "Force reflecting bilateral control of master–slave systems in teleoperation," *J. Intell. Robot. Syst.* **52**(2), 209–232 (2008).

14. L. Mohammadi, A. Alfi and B. Xu, "Robust bilateral control for state convergence in uncertain teleoperation systems with time-varying delay: A guaranteed cost control design," *Nonlinear Dyn.* **88**(2), 1413–1426 (2017).
15. R. Aracil *et al.*, "Bilateral control by state convergence based on transparency for systems with time delay," *Robotics Auton. Syst.* **61**(2), 86–94 (2013).
16. A. Alfi *et al.* "Design and implementation of robust-fixed structure controller for telerobotic systems," *J. Intell. Robot. Syst.* **83**(2), 253–269 (2016).
17. N. Chopra, M. W. Spong, R. Ortega and N. E. Barabanov, "On tracking performance in bilateral teleoperation," *IEEE Trans. Robot.* **22**(4), 861–866 (2006).
18. N. Chopra, P. Berestesky and M. W. Spong, 'Bilateral teleoperation over unreliable communication networks," *IEEE Trans. Control Syst. Technol.* **16**(2), 304–313 (2008).
19. D. Lee and M. W. Spong, "Passive bilateral teleoperation with constant time delay," *IEEE Trans. Robot.* **22**(2), 269–281 (2006).
20. E. Nuño, "Haptic Guidance with Force Feedback to Assist Teleoperation Systems Via High Speed Networks," *Proceedings of the IEEE International Symposium on Robotics* (2006) pp. 1–14.
21. E. Nuño, R. Ortega, N. Barabanov and L. Basañez, "A globally stable PD controller for bilateral teleoperators," *IEEE Trans. Robot.* **24**(3), 753–758 (2008).
22. E. Nuño, L. Basañez and R. Ortega, "Passivity-based control for bilateral teleoperation: A tutorial," *Automatica* **47**, 485–495 (2011).
23. Z. Li, L. Ding, H. Gao, G. Duan and C. Y. Su, "Trilateral teleoperation of adaptive fuzzy force/motion control for nonlinear teleoperators with communication random delays," *IEEE Trans. Fuzzy Syst.* **21**(4), 610–624 (2013).
24. Z. Li and C. Y. Su, "Neural-adaptive control of single-master–multiple-slaves teleoperation for coordinated multiple mobile manipulators with time-varying communication delays and input uncertainties," *IEEE Trans. Neural Netw. Learn. Syst.* **24**(9), 1400–1413 (2013).
25. Z. Li, X. Cao and N. Ding, "Adaptive fuzzy control for synchronization of nonlinear teleoperators with stochastic time-varying communication delays," *IEEE Trans. Fuzzy Syst.* **19**(4), 745–757 (2011).
26. Z. Lu, P. Huang and Z. Liu, "Predictive approach for sensorless bimanual teleoperation under random time delays with adaptive fuzzy control," *IEEE Trans. Ind. Electron.* **65**(3), 2439–2448 (2018).
27. Z. Zhao, P. Huang, Z. Lu and Z. Liu, "Augmented reality for enhancing tele-robotic system with force feedback," *Robot. Auton. Syst.* **96**, 93–101 (2017).
28. P. Desbats, F. Geffard, G. Piolain and A. Coudray, "Force-feedback teleoperation of an industrial robot in a nuclear spent fuel reprocessing plant," *Ind. Robot* **33**(3), 178–186 (2006).
29. S. Soyguder and T. Abut, "Haptic industrial robot control with variable time delayed bilateral teleoperation," *Ind. Robot* **43**(4), 390–402 (2016).
30. B. Khademian and K. Hashtrudi-Zaad, "A framework for unconditional stability analysis of multimaster/multislave teleoperation systems," *IEEE Trans. Robot.* **29**(3), 684–694 (2013).
31. K. Razi and K. Hashtrudi-Zaad, "Analysis of coupled stability in multilateral dual-user teleoperation systems," *IEEE Trans. Robot.* **30**(3), 631–641 (2014).
32. J. Li, M. Tavakoli and Q. Huang, "Absolute stability of multi-dof multilateral haptic systems," *IEEE Trans. Control Syst. Technol.* **22**(6), 2319–2328 (2014).
33. Z. Lu *et al.,* "Enhanced transparency dual-user shared control teleoperation architecture with multiple adaptive dominance factors," *Int. J. Control. Autom. Syst.* **15**(5), 2301–2312 (2017).
34. J. E. Colgate, M. C. Stanley and J. M. Brown, "Issues in the Haptic Display of Tool Use," *Proceedings of the IEEE/RSJ International Conference on Intelligent Robots and Systems* (1995) pp. 140–145.
35. C. B. Zilles and J. K. Salisbury, "A constraint-based god-object method for haptic display," *Proceedings of the IEEE/RSJ International Conference on Intelligent Robots and Systems* (1995) pp. 146–151.
36. B. M. Howard and J. M. Vance, "Desktop haptic virtual assembly using physically based modelling," *Virtual Reality* **11**(4), 207–215 (2007).
37. X. Hou and O. Sourina, "Stable adaptive algorithm for six degrees-of-freedom haptic rendering in a dynamic environment," *Vis. Comput.* **29**(10), 1063–1075 (2013).
38. Blender, "https://www.blender.org/" (2017).
39. S. Arimoto and F. Miyazaki, "Stability and Robustness of PID Feedback Control for Robot Manipulators of Sensory Capability," *Proceedings of the International Symposium on Robotics Research* (1984) pp. 783–799.
40. W. Khalil and E. Dombre, "Modeling, identification and control of robots," Kogan Page Science Paper Edition, Butterworth-Heinemann (2004). ISBN-10: 190399666X
41. E. Nuño, L. Basañez and M. Prada, "Asymptotic Stability of Teleoperators with Variable Time-Delays," *Proceedings of the IEEE International Conference on Robotics and Automation* (2009) pp. 4332–4337.
42. E. Nuño, L. Basañez, R. Ortega and M. W. Spong, "Position tracking for non-linear teleoperators with variable time Delay," *Int. J. Robot. Res.* **28**(7), 895–910 (2009).
43. C. C. Hua and X. P. Liu, "Delay-dependent stability criteria of teleoperation systems with asymmetric time-varying delays," *IEEE Trans. Robot.* **26**(5), 895–910 (2010).
44. J. J. E. Slotine and W. Li, *Applied Nonlinear Control* (Prentice Hall, 1991).
45. D. Lawrence, "Stability and transparency in bilateral teleoperation," *IEEE Trans. Robot. Autom.* **9**(5), 624–637 (1993).
46. P. F. Hokayem and M. W. Spong, "Bilateral teleoperation: An historical survey," *Automatica* **42**(12), 2035–2057 (2006).

47. Stäubli Technical Documentation Interactive CD-ROM, "Arm–RX series 160 family Instruction Manual" (2008).

Appendix: Proof of the Lyapunov stability

The first time derivative of the Lyapunov function candidate with (P3) and (P4) can be written as follows:

$$\begin{aligned}\dot{V} = {} & \dot{\underline{q}}_m{}^T \left(C_m + C_m{}^T\right) \dot{\underline{q}}_m + 2\dot{\underline{q}}_m{}^T \left(\underline{\tau}_m - \underline{\tau}_{\text{user}} - C_m \dot{\underline{q}}_m\right) + \dot{\underline{q}}_b{}^T \left(C_b + C_b{}^T\right) \dot{\underline{q}}_b \\ & + 2\dot{\underline{q}}_b{}^T \left(\underline{\tau}_b - C_b \dot{\underline{q}}_b\right) + \frac{K_m}{K_s} \dot{\underline{q}}_s{}^T \left(C_s + C_s{}^T\right) \dot{\underline{q}}_s + 2\frac{K_m}{K_s} \dot{\underline{q}}_s{}^T \left(\underline{\tau}_s + \underline{F}_e - C_s \dot{\underline{q}}_s\right) \\ & - 2K_m \dot{\underline{q}}_m^T \left(\underline{q}_m - \underline{q}_b\right) + 2K_m \dot{\underline{q}}_b^T \left(\underline{q}_m - \underline{q}_b\right) + 2K_m \dot{\underline{q}}_b^T \left(\underline{q}_b - \underline{q}_s\right) \\ & - 2K_m \dot{\underline{q}}_s^T \left(\underline{q}_b - \underline{q}_s\right) - 2\dot{\underline{q}}_m^T \underline{\tau}_{\text{user}} - 2\frac{K_m}{K_s} \dot{\underline{q}}_s^T \underline{f}_e - B_m \left(\dot{\underline{q}}_b^T \dot{\underline{q}}_b - \dot{\underline{q}}_b^T (t - T_1) \dot{\underline{q}}_b (t - T_1)\right) \\ & + \frac{K_m}{K_s} B_s \left(\dot{\underline{q}}_b^T \dot{\underline{q}}_b - \dot{\underline{q}}_b^T (t - T_2) \dot{\underline{q}}_b (t - T_2)\right) + \overline{T}_1 \dot{\underline{q}}_b^T S \dot{\underline{q}}_b \\ & - \int_{t-\overline{T}_1}^{t} \dot{\underline{q}}_b^T (\sigma) S \dot{\underline{q}}_b (\sigma)\, \mathrm{d}\sigma + \overline{T}_2 \dot{\underline{q}}_b^T Z \dot{\underline{q}}_b - \int_{t-\overline{T}_2}^{t} \dot{\underline{q}}_b^T (\sigma) Z \dot{\underline{q}}_b (\sigma)\, \mathrm{d}\sigma \end{aligned} \tag{A1}$$

(A1) can be rearranged as follows:

$$\begin{aligned}\dot{V} = {} & 2\dot{\underline{q}}_m^T \left(\underline{\tau}_m - \underline{\tau}_{\text{user}}\right) + 2\dot{\underline{q}}_b^T \underline{\tau}_b + 2\frac{K_m}{K_s} \dot{\underline{q}}_s^T \left(\underline{\tau}_s + \underline{F}_e\right) + 2K_m \left(\dot{\underline{q}}_b^T - \dot{\underline{q}}_m^T\right) \left(\underline{q}_m - \underline{q}_b\right) \\ & + 2K_m \left(\dot{\underline{q}}_b^T - \dot{\underline{q}}_s^T\right) \left(\underline{q}_b - \underline{q}_s\right) - 2\dot{\underline{q}}_m^T \underline{\tau}_{\text{user}} - 2\frac{K_m}{K_s} \dot{\underline{q}}_s^T \underline{f}_e \\ & - B_m \left(\dot{\underline{q}}_b^T \dot{\underline{q}}_b - \dot{\underline{q}}_b^T (t - T_1) \dot{\underline{q}}_b (t - T_1)\right) + \frac{K_m}{K_s} B_s \left(\dot{\underline{q}}_b^T \dot{\underline{q}}_b - \dot{\underline{q}}_b^T (t - T_2) \dot{\underline{q}}_b (t - T_2)\right) \\ & + \overline{T}_1 \dot{\underline{q}}_b^T S \dot{\underline{q}}_b - \int_{t-\overline{T}_1}^{t} \dot{\underline{q}}_b^T (\sigma) S \dot{\underline{q}}_b (\sigma)\, \mathrm{d}\sigma + \overline{T}_2 \dot{\underline{q}}_b^T Z \dot{\underline{q}}_b - \int_{t-\overline{T}_2}^{t} \dot{\underline{q}}_b^T (\sigma) Z \dot{\underline{q}}_b (\sigma)\, \mathrm{d}\sigma \end{aligned} \tag{A2}$$

Substituting the above given expressions and bounds of $\underline{\tau}_m$, $\underline{\tau}_b$ and $\underline{\tau}_s$:

$$\begin{aligned}\dot{V} = {} & 2K_m \dot{\underline{q}}_m^T \left(\underline{q}_m - \underline{q}_b(t - T_1)\right) + 2B_m \dot{\underline{q}}_m^T \left(\dot{\underline{q}}_m - \dot{\underline{q}}_b(t - T_1)\right) + 2\dot{\underline{q}}_m^T \underline{f}_e\,(t - T_3) \\ & - 2\dot{\underline{q}}_m^T \underline{\tau}_{\text{user}} + 2\dot{\underline{q}}_b^T \underline{\tau}_b + 2K_m \dot{\underline{q}}_s^T \left(\underline{q}_b\,(t - T_2) - \underline{q}_s\right) + 2\frac{K_m}{K_s} B_s \dot{\underline{q}}_s^T \left(\dot{\underline{q}}_b\,(t - T_2) - \dot{\underline{q}}_s\right) \\ & + 2\frac{K_m}{K_s} \dot{\underline{q}}_s^T \underline{f}_e + 2K_m \left(\dot{\underline{q}}_b^T - \dot{\underline{q}}_m^T\right) \left(\underline{q}_m - \underline{q}_b\right) + 2K_m \left(\dot{\underline{q}}_b^T - \dot{\underline{q}}_s^T\right) \left(\underline{q}_b - \underline{q}_s\right) \\ & - 2\dot{\underline{q}}_m^T \underline{\tau}_{\text{user}} - 2\frac{K_m}{K_s} \dot{\underline{q}}_s^T \underline{f}_e - B_m \left(\dot{\underline{q}}_b^T \dot{\underline{q}}_b - \dot{\underline{q}}_b^T (t - T_1) \dot{\underline{q}}_b (t - T_1)\right) \\ & + \frac{K_m}{K_s} B_s \left(\dot{\underline{q}}_b^T \dot{\underline{q}}_b - \dot{\underline{q}}_b^T (t - T_2) \dot{\underline{q}}_b (t - T_2)\right) + \overline{T}_1 \dot{\underline{q}}_b^T S \dot{\underline{q}}_b \\ & - \int_{t-\overline{T}_1}^{t} \dot{\underline{q}}_b^T (\sigma) S \dot{\underline{q}}_b (\sigma)\, \mathrm{d}\sigma + \overline{T}_2 \dot{\underline{q}}_b^T Z \dot{\underline{q}}_b - \int_{t-\overline{T}_2}^{t} \dot{\underline{q}}_b^T (\sigma) Z \dot{\underline{q}}_b (\sigma)\, \mathrm{d}\sigma \end{aligned} \tag{A3}$$

https://doi.org/10.1017/S0263574718001042 Published online by Cambridge University Press

Manipulating (A3) by adding and subtracting $\underline{q}_b$ into the first and sixth terms, it can be rearranged as follows:

$$\begin{aligned}\dot{V} = {} & 2K_m\underline{\dot{q}}_m^T\left(\underline{q}_b - \underline{q}_b(t-T_1)\right) + 2B_m\underline{\dot{q}}_m^T\left(\underline{\dot{q}}_m - \underline{\dot{q}}_b(t-T_1)\right) + 2\underline{\dot{q}}_m^T\underline{f}_e(t-T_3) \\ & - 2\underline{\dot{q}}_m^T\underline{\tau}_{\text{user}} + 2\underline{\dot{q}}_b^T\underline{\tau}_b + 2K_m\underline{\dot{q}}_s^T\left(\underline{q}_b(t-T_2) - \underline{q}_b\right) + 2\frac{K_m}{K_s}B_s\underline{\dot{q}}_s^T\left(\underline{\dot{q}}_b(t-T_2) - \underline{\dot{q}}_s\right) \\ & + 2\frac{K_m}{K_s}\underline{\dot{q}}_s^T\underline{f}_e + 2K_m\underline{\dot{q}}_b^T\left(\underline{q}_m - \underline{q}_s\right) - 2\underline{\dot{q}}_m^T\underline{\tau}_{\text{user}} - 2\frac{K_m}{K_s}\underline{\dot{q}}_s^T\underline{f}_e \\ & - B_m\left(\underline{\dot{q}}_b^T\underline{\dot{q}}_b - \underline{\dot{q}}_b^T(t-T_1)\underline{\dot{q}}_b(t-T_1)\right) + \frac{K_m}{K_s}B_s\left(\underline{\dot{q}}_b^T\underline{\dot{q}}_b - \underline{\dot{q}}_b^T(t-T_2)\underline{\dot{q}}_b(t-T_2)\right) \\ & + \overline{T}_1\underline{\dot{q}}_b^TS\underline{\dot{q}}_b - \int_{t-\overline{T}_1}^{t}\underline{\dot{q}}_b^T(\sigma)S\underline{\dot{q}}_b(\sigma)\,\mathrm{d}\sigma + \overline{T}_2\underline{\dot{q}}_b^TZ\underline{\dot{q}}_b - \int_{t-\overline{T}_2}^{t}\underline{\dot{q}}_b^T(\sigma)Z\underline{\dot{q}}_b(\sigma)\,\mathrm{d}\sigma \end{aligned} \tag{A4}$$

Taking into account the following equality:

$$\underline{q}_i(t-T) - \underline{q}_i = \int_0^T \underline{\dot{q}}_i(t-\sigma)\mathrm{d}\sigma$$

and expanding the second and seventh terms:

$$\begin{aligned}\dot{V} = {} & 2K_m\underline{\dot{q}}_m^T\int_{t-T_1}^{t}\underline{\dot{q}}_b(\sigma)\mathrm{d}\sigma + 2B_m\underline{\dot{q}}_m^T\underline{\dot{q}}_m - 2B_m\underline{\dot{q}}_m^T\underline{\dot{q}}_b(t-T_1) + 2\underline{\dot{q}}_m^T\underline{f}_e(t-T_3) \\ & - 2\underline{\dot{q}}_b^T\underline{\tau}_{\text{user}} + 2\underline{\dot{q}}_m^T\underline{\tau}_b + 2\frac{K_m}{K_s}\underline{\dot{q}}_s^T\underline{f}_e + 2K_m\underline{\dot{q}}_s^T\int_{t-T_2}^{t}\underline{\dot{q}}_b(\sigma)\,\mathrm{d}\sigma + 2\frac{K_m}{K_s}B_s\underline{\dot{q}}_s^T\underline{\dot{q}}_b(t-T_2) \\ & - 2\frac{K_m}{K_s}B_s\underline{\dot{q}}_s^T\underline{\dot{q}}_s + 2K_m\underline{\dot{q}}_b^T\left(\underline{q}_m - \underline{q}_s\right) - 2\underline{\dot{q}}_m^T\underline{\tau}_{\text{user}} - 2\frac{K_m}{K_s}\underline{\dot{q}}_s^T\underline{f}_e \\ & - B_m\left(\underline{\dot{q}}_b^T\underline{\dot{q}}_b - \underline{\dot{q}}_b^T(t-T_1)\underline{\dot{q}}_b(t-T_1)\right) + \frac{K_m}{K_s}B_s\left(\underline{\dot{q}}_b^T\underline{\dot{q}}_b - \underline{\dot{q}}_b^T(t-T_2)\underline{\dot{q}}_b(t-T_2)\right) \\ & + \overline{T}_1\underline{\dot{q}}_b^TS\underline{\dot{q}}_b - \int_{t-\overline{T}_1}^{t}\underline{\dot{q}}_b^T(\sigma)S\underline{\dot{q}}_b(\sigma)\,\mathrm{d}\sigma + \overline{T}_2\underline{\dot{q}}_b^TZ\underline{\dot{q}}_b - \int_{t-\overline{T}_2}^{t}\underline{\dot{q}}_b^T(\sigma)Z\underline{\dot{q}}_b(\sigma)\,\mathrm{d}\sigma \end{aligned} \tag{A5}$$

Applying the following bound:

$$2\underline{\dot{q}}_i\underline{\dot{q}}_j(t-T) \le \underline{\dot{q}}_i^T\underline{\dot{q}}_i + \underline{\dot{q}}_j^T(t-T)\underline{\dot{q}}_j(t-T)$$

to the third and ninth terms of (A5):

$$\begin{aligned}\dot{V} = {} & 2K_m\underline{\dot{q}}_m^T\int_{t-T_1}^{t}\underline{\dot{q}}_b(\sigma)\mathrm{d}\sigma + 2B_m\underline{\dot{q}}_m^T\underline{\dot{q}}_m - B_m\underline{\dot{q}}_m^T\underline{\dot{q}}_m - B_m\underline{\dot{q}}_b^T(t-T_1)\underline{\dot{q}}_b(t-T_1) \\ & + 2\underline{\dot{q}}_m^T\underline{f}_e(t-T_2) - 2\underline{\dot{q}}_m^T\underline{\tau}_{\text{user}} + 2\underline{\dot{q}}_b^T\underline{\tau}_b + 2\frac{K_m}{K_s}\underline{\dot{q}}_s^T\underline{f}_e + 2K_m\underline{\dot{q}}_s^T\int_{t-T_2}^{t}\underline{\dot{q}}_b(\sigma)\,\mathrm{d}\sigma \\ & + \frac{K_m}{K_s}B_s\underline{\dot{q}}_s^T\underline{\dot{q}}_s + \frac{K_m}{K_s}\underline{\dot{q}}_b^T(t-T_2)\underline{\dot{q}}_b(t-T_2) - 2\frac{K_m}{K_s}B_s\underline{\dot{q}}_s^T\underline{\dot{q}}_s + 2K_m\underline{\dot{q}}_b^T\left(\underline{q}_m - \underline{q}_s\right) \end{aligned}$$

https://doi.org/10.1017/S0263574718001042 Published online by Cambridge University Press

$$
\begin{aligned}
&- 2\dot{\underline{q}}_m^T \underline{\tau}_{\text{user}} - 2\frac{K_m}{K_s}\dot{\underline{q}}_s^T \underline{f}_e - B_m\left(\dot{\underline{q}}_b^T \underline{\dot{q}}_b - \dot{\underline{q}}_b^T (t-T_1)\,\underline{\dot{q}}_b (t-T_1)\right) \\
&+ \frac{K_m}{K_s} B_s\left(\dot{\underline{q}}_b^T \underline{\dot{q}}_b - \dot{\underline{q}}_b^T (t-T_2)\,\underline{\dot{q}}_b (t-T_2)\right) + \overline{T}_1 \dot{\underline{q}}_b^T S \underline{\dot{q}}_b \\
&- \int_{t-\overline{T}_1}^{t} \dot{\underline{q}}_b^T (\sigma)\, S \underline{\dot{q}}_b (\sigma)\, \mathrm{d}\sigma + \overline{T}_2 \dot{\underline{q}}_b^T Z \underline{\dot{q}}_b - \int_{t-\overline{T}_2}^{t} \dot{\underline{q}}_b^T (\sigma)\, Z \underline{\dot{q}}_b (\sigma)\, \mathrm{d}\sigma
\end{aligned} \tag{A6}
$$

(A6) can be simplified and rearranged as follows:

$$
\begin{aligned}
\dot{V} = {} & 2K_m \dot{\underline{q}}_m^T \int_{t-T_1}^{t} \underline{\dot{q}}_b(\sigma)\mathrm{d}\sigma + B_m \dot{\underline{q}}_m^T \underline{\dot{q}}_m + 2\dot{\underline{q}}_m^T \underline{f}_e\,(t-T_3) - 2\dot{\underline{q}}_m^T \underline{\tau}_{\text{user}} + 2\dot{\underline{q}}_b^T \underline{\tau}_b \\
& + 2\frac{K_m}{K_s}\dot{\underline{q}}_s^T \underline{f}_e + 2K_m \dot{\underline{q}}_s^T \int_{t-T_2}^{t} \underline{\dot{q}}_b\,(\sigma)\,\mathrm{d}\sigma - \frac{K_m}{K_s} B_s \dot{\underline{q}}_s^T \underline{\dot{q}}_s + 2K_m \dot{\underline{q}}_b^T \left(\underline{q}_m - \underline{q}_s\right) \\
& - 2\dot{\underline{q}}_m^T \underline{\tau}_{\text{user}} - 2\frac{K_m}{K_s}\dot{\underline{q}}_s^T \underline{f}_e + (\frac{K_m}{K_s} B_s - B_m)\dot{\underline{q}}_b^T \underline{\dot{q}}_b + \overline{T}_1 \dot{\underline{q}}_b^T S \underline{\dot{q}}_b \\
& - \int_{t-\overline{T}_1}^{t} \dot{\underline{q}}_b^T (\sigma)\, S \underline{\dot{q}}_b (\sigma)\, \mathrm{d}\sigma + \overline{T}_2 \dot{\underline{q}}_b^T Z \underline{\dot{q}}_b - \int_{t-\overline{T}_2}^{t} \dot{\underline{q}}_b^T (\sigma)\, Z \underline{\dot{q}}_b (\sigma)\, \mathrm{d}\sigma
\end{aligned} \tag{A7}
$$

Following inequalities are based on the Lemma 1:

$$
2K_m \dot{\underline{q}}_m^T \int_{t-T_1}^{t} \underline{\dot{q}}_b\,(\sigma)\,\mathrm{d}\sigma - \int_{t-T_1}^{t} \dot{\underline{q}}_b^T (\sigma)\, S \underline{\dot{q}}_b (\sigma)\, \mathrm{d}\sigma \le \overline{T}_1 {K_m}^2 \dot{\underline{q}}_m^T S^{-1} \underline{\dot{q}}_m \tag{A8}
$$

$$
2K_m \dot{\underline{q}}_s^T \int_{t-T_2}^{t} \underline{\dot{q}}_b\,(\sigma)\,\mathrm{d}\sigma - \int_{t-T_2}^{t} \dot{\underline{q}}_b^T (\sigma)\, Z \underline{\dot{q}}_b (\sigma)\, \mathrm{d}\sigma \le \overline{T}_2 {K_m}^2 \dot{\underline{q}}_s^T Z^{-1} \underline{\dot{q}}_s \tag{A9}
$$

Substituting (A8) and (A9) into (A7) and rearranging

$$
\begin{aligned}
\dot{V} = {} & \dot{\underline{q}}_m^T \left(\overline{T}_1 {K_m}^2 S^{-1} + B_m\right) \underline{\dot{q}}_m + \dot{\underline{q}}_b^T \left(\overline{T}_1 S + \overline{T}_2 Z + \frac{K_m}{K_s} B_s - B_m\right) \underline{\dot{q}}_b \\
& + \dot{\underline{q}}_s^T \left(\overline{T}_2 {K_m}^2 Z^{-1} - \frac{K_m}{K_s} B_s\right) \underline{\dot{q}}_s + 2\dot{\underline{q}}_m^T (\underline{f}_e\,(t-T_3) - 2\underline{\tau}_{\text{user}}) + 2\dot{\underline{q}}_b^T (K_m \left(\underline{q}_m - \underline{q}_s\right) + \underline{\tau}_b)
\end{aligned} \tag{A10}
$$

With the conditions given by (15) for the last two terms of the (A10), and with the following inequalities being satisfied:

$$
\overline{T}_1 {K_m}^2 S^{-1} + B_m \le 0
$$

$$
\overline{T}_1 S + \overline{T}_2 Z + \frac{K_m}{K_s} B_s - B_m \le 0
$$

$$
\overline{T}_2 {K_m}^2 Z^{-1} - \frac{K_m}{K_s} B_s \le 0
$$

the expression (A10) shows the negative semi-definiteness of $\dot{V}$, implying the boundedness of $\underline{\dot{q}}_i$ and $\underline{q}_m - \underline{q}_s$, and hence the Lyapunov stability of the proposed bilateral haptic loop.

https://doi.org/10.1017/S0263574718001042 Published online by Cambridge University Press